


RESEARCH

Open Access



# Automatic and continuous blood pressure monitoring via an optical-fiber-sensor-assisted smartwatch

Liangye Li<sup>1</sup>, Shunfeng Sheng<sup>1</sup>, Yunfei Liu<sup>1</sup>, Jianpei Wen<sup>2</sup>, Changying Song<sup>1</sup>, Zhipeng Chen<sup>1</sup>, Wangyang Xu<sup>1</sup>, Zhi Zhang<sup>1</sup>, Wei Fan<sup>3</sup>, Chen Chen<sup>2</sup>, Qizhen Sun<sup>1,4\*</sup>  and Perry-Ping Shum<sup>5\*</sup>

\*Correspondence:  
qzsun@mail.hust.edu.cn.cn;  
shenp@sustech.edu.cn

<sup>1</sup> School of Optical and Electronic Information, National Engineering Research Center for Next Generation Internet Access System (NGIA), Huazhong University of Science and Technology, Wuhan 430074, China

<sup>2</sup> Hubei Key Laboratory of Genetics and Molecular Mechanisms of Cardiometabolic Disorders, Division of Cardiology, Huazhong University of Science and Technology, Tongji Medical College, Tongji Hospital, Wuhan 430074, China

<sup>3</sup> Huawei Technologies Co, Ltd, Shenzhen 218129, China

<sup>4</sup> Huazhong University of Science and Technology, HUST-Wuxi Research Institute, Wuxi 214174, China

<sup>5</sup> Department of Electrical and Electronic Engineering, Southern University of Science and Technology, Shenzhen 518055, China

## Abstract

Automatic and continuous blood pressure monitoring is important for preventing cardiovascular diseases such as hypertension. The evaluation of medication effects and the diagnosis of clinical hypertension can both benefit from continuous monitoring. The current generation of wearable blood pressure monitors frequently encounters limitations with inadequate portability, electrical safety, limited accuracy, and precise position alignment. Here, we present an optical fiber sensor-assisted smartwatch for precise continuous blood pressure monitoring. A fiber adapter and a liquid capsule were used in the building of the blood pressure smartwatch based on an optical fiber sensor. The fiber adapter was used to detect the pulse wave signals, and the liquid capsule was used to expand the sensing area as well as the conformability to the body. The sensor holds a sensitivity of  $-213\mu\text{w/kPa}$ , a response time of 5 ms, and high reproducibility with 70,000 cycles. With the assistance of pulse wave signal feature extraction and a machine learning algorithm, the smartwatch can continuously and precisely monitor blood pressure. A wearable smartwatch featuring a signal processing chip, a Bluetooth transmission module, and a specially designed cellphone APP was also created for active health management. The performance in comparison with commercial sphygmomanometer reference measurements shows that the systolic pressure and diastolic pressure errors are  $-0.35 \pm 4.68$  mmHg and  $-2.54 \pm 4.07$  mmHg, respectively. These values are within the acceptable ranges for Grade A according to the British Hypertension Society (BHS) and the Association for the Advancement of Medical Instrumentation (AAMI). The smartwatch assisted with an optical fiber is expected to offer a practical paradigm in digital health.

**Keywords:** Blood pressure, Optical fiber sensor, Smartwatch

## Introduction

The most prevalent disease worldwide has been hypertension, which dramatically raises the chance of developing heart, brain, kidney, and other disorders [1–4]. In the past three decades, 1.28 billion persons aged 30–79 who have hypertension are now affected by it, but only 14% have it under control [5]. It has been reported that monitoring blood pressure fluctuations within 24 h will contribute to assessing drug effects and preventing

cardiovascular diseases. As such, continuous blood pressure monitoring is in great demand for cardiovascular health management.

Traditional cuff sphygmomanometers require a cuff airbag wrapped around the arm to inflate and pressurize [6, 7]. The inflated airbag interrupts the blood flow and further limits the possibility of continuous measurement. To achieve wearable continuous blood pressure monitoring, photoplethysmogram (PPG) and pressure/strain sensors have been widely developed. PPG measures the light attenuation due to the blood flow, records the pulsatile state of blood vessels, and obtains pulse wave signals which are essential for blood pressure estimation [8–10]. Despite the potential of PPG sensors for non-invasive and continuous ways, the large power consumption, and low sensitivity constrained its application in clinical practice. Recently, benefiting from the development of electronics, materials, and mechanical designs, numerous flexible biomedical sensors such as those based on triboelectric [11, 12], piezoelectric [13], magnetoelastic [14], resistive [15, 16], capacitive [17, 18], and ultrasonic technology [19], have been created to constantly monitor pulse wave signals and blood pressure. Although the above sensors have already shown promise for sensing physiological signals, the sensitivity to electromagnetic interferences (EMIs) and un-insulation become new barriers to the broad adoption of this technology in practice [20]. In addition, obstacles to the practical application include the biocompatibility of metallic components. Therefore, the development of a highly sensitive flexible blood pressure sensor with the ability of electrical safety is urgent in an intelligent wearable device.

Nowadays, optical fiber sensors have offered avenues for blood pressure monitoring. They hold considerable promise for wearable applications due to their high sensitivity, flexibility, fast response time, lightweight, compactness, great biocompatibility, and immunity to electromagnetic interference [21–23]. Moreover, under the background of Fiber To The Home (FTTH), more details regarding cardiovascular health can be obtained using optical fiber sensors in network systems, which is important for future medical networks and the realization of telemedicine and precision [24]. Recent advances based on micro-fiber [25], Fiber Bragg Gratings (FBG) [26], and Singlemode-Multimode-Singlemode (SMS) [27] have been widely reported. Despite the great performance the reported sensors exhibit, there remains space to be improved. The current optical fiber sensor greatly depends on the position of the sensor alignment to the artery, which is not amenable for practice. In addition, the aforementioned blood pressure sensors estimate systolic and diastolic pressure through pulse transit time (PTT). Nevertheless, due to the confounding influences of the cardiovascular, pulmonary, and autonomic nervous systems, the association between PTT and blood pressure is not linear and has low accuracy. Last but not least, the complex and bulky optical fiber blood pressure monitoring systems make it difficult to be integrated a continuous monitoring smartwatch. In summary, it has not yet been possible to create devices that are very sensitive, naturally electrically safe, and devoid of position alignment.

In this work, we proposed and developed an optical fiber sensor-assisted smartwatch for continuous precise blood pressure monitoring. A fiber adapter and a liquid capsule were used in the building of the blood pressure smartwatch. The fiber adapter was used to detect the pulse wave signals and the liquid capsule was used to enhance the sensing area as well as the conformability to the body. Then, typical features of pulse

wave signals will be extracted and constructed blood pressure estimation model with a machine learning algorithm. The optical fiber sensor facilitates the smartwatch to have a high sensitivity up to  $-213 \mu\text{w}/\text{kPa}$  in the pressure range of 0–2 kPa, an ultra-fast response time of 5 ms, and high reproducibility with 70,000 cycles. In addition, a wearable signal processing chip, a Bluetooth transmission module, and a specially designed mobile APP are easily connected with the optical fiber sensor to create a blood pressure monitoring smartwatch. The smartwatch's performance reveals that the mean deviation is less than 3 mmHg and the error standard deviation is less than 5 mmHg, which meets the requirement of the international standard. In order to solve the problem of pulse shape variation and the difficulty to extract the feature points uniformly, the automatic correction threshold method is proposed in this work. The Feature extraction based on automatic correction thresholding method will improve the accuracy of feature recognition, and further increase the accuracy of blood pressure. Our smartwatch allows for precise continuous blood pressure monitoring, illustrating its potential application in cardiovascular disease prevention and diagnosis, which will facilitate the development of individual-centered health management.

## Method

### Continuous blood pressure monitoring smartwatch

To provide tailored healthcare delivery and encourage anticipatory behavior with an emphasis on illness prevention and health promotion, an optical fiber sensor assisted smartwatch was designed for continuous and portable blood pressure monitoring. A schematic of the blood pressure monitoring system is displayed in Fig. 1(a). The system consisted of an optical fiber sensor, signal acquisition, data processing, blood pressure calculation, smartwatch terminal, and cellphone. The heart's pulsation propagates outward along arterial vessels to create the pulse wave. The pulsation will result in different patterns corresponding to artery elasticity, and blood viscosity. The pulse signals were sensed by the optical fiber sensor and then detected by photodetectors and converted into electrical signals. The microprocessor was designed which included signal acquisition, conversion, denoising, and feature extraction. In order to estimate blood pressure more accurately, the neural network was used here to train the model. Finally, the systolic blood pressure (SBP) and diastolic blood pressure (DBP) values were displayed on the screen and transmitted to a mobile phone wirelessly.

### Principle and fabrication of optical fiber sensor-assisted smartwatch

An optical fiber sensor-based blood pressure smartwatch is made up of two components: a liquid capsule and a fiber adaptor. The fiber adapter was used to collect weak pressure signals, such as pulse wave signals, the liquid capsule was utilized to expand the sensing area. Figure 1(b) exhibits the whole structure of the proposed fiber adapter which comprised a polyethylene (PE) tube (inner/outer diameter: 127/254  $\mu\text{m}$ , SCI PE-01), an air core, and two multimode fibers. It should be pointed out that the two multimode fibers had the same cladding diameter while different core diameters (Sending MMF, core/cladding: 62.5/125  $\mu\text{m}$ , Receiving MMF, core/cladding: 105/125  $\mu\text{m}$ ). To improve the stability, ultraviolet (UV) glue was chosen to seal the two multimode fibers and PE tube at both ends because of its rapid curing.

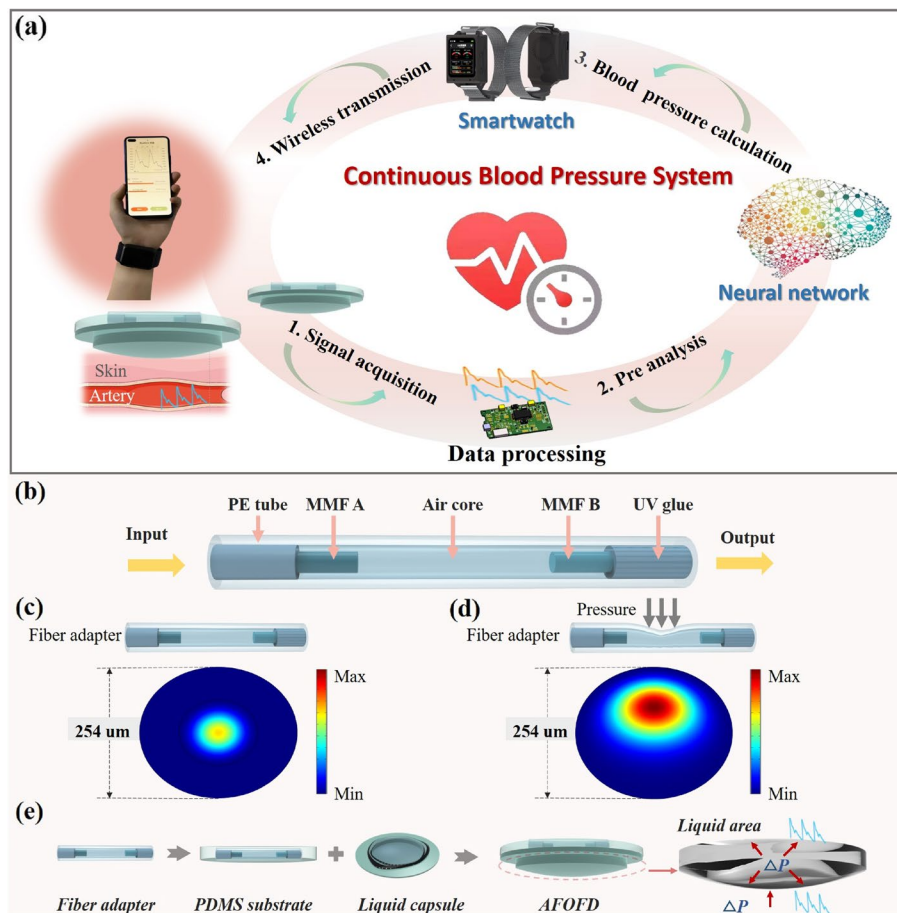


**Fig. 1** Schematic of the blood pressure monitoring system. **a** The monitoring system consists of an optical fiber sensor, signal acquisition, data processing, blood pressure calculation, smartwatch terminal, and mobile phone. **b** The fiber adapter's construction. **c** Distribution of the field energy density. **d** Distribution of the optical field energy density under pressure **e** The fabrication of proposed sensor

In order to understand the working principle of fiber adapter, finite-element analysis (FEA) by Comsol Multiphysics simulating the optical field energy of two adapters against increasing external pressure was conducted. As demonstrated in Fig. 1 (c), when probe light passed through the Sending MMF and entered the PE tube without being compressed, the majority of the optical field energy was distributed in the air core. Figure 1 (d) illustrates that the PE tube would deform when pressure was applied, the transmission loss was caused by the optical field's energy distribution, which tended to the cladding. As such, by monitoring the change in transmitted light intensity at the receiving end, pulse wave signals can be measured to estimate blood pressure.

Although fiber adapter has already shown excellent promise for micro-scale vital signs signals, distortion caused by position drift and misalignment remain barriers to broad adoption of this technology in practical application. For achieving free alignment and spatial insensitivity, a liquid capsule was designed. According to Pascal's Principle, any location in an incompressible static fluid that is stimulated by an external pressure may experience a rise in pressure, which will instantly be communicated to all other places in the static fluid [28]. As such, the fiber adapter sealed inside the capsule will receive any

detected pulse wave signals from the liquid capsule base without degradation so that the spatial insensitivity and free alignment are successfully realized. In addition, the liquid capsule which promotes conformability to the body will improve the coupling between the optical fiber sensor and body, enabling more precise blood pressure monitoring.

The process for fabrication of optical fiber sensor is shown in Fig. 1(e). First, the two multimode fibers with flat end surfaces were aligned and inserted into both sides of the PE tube. For better stability, the two multimode fibers and PE tubes were sealed by ultraviolet (UV) glue. Next, the Polydimethylsiloxane (PDMS, Sylgard 184; module,  $\approx 2$  MPa) films with a thickness of 700  $\mu\text{m}$  were used as the packaging material which sandwiched the fiber adapter. Here, PDMS was chosen owing to its low refractive index, excellent flexibility, transparency, and biocompatibility [29–31]. As for the liquid capsule, the PDMS foundation and liquid made up the convex-shaped liquid capsule, which had a 25 mm radius of curvature. The PDMS base had an external diameter of 20 mm, a depth of 1.75 mm, and a thickness of 400  $\mu\text{m}$ . The recessed area (depth: 1.5 mm, diameter 15 mm) in the middle was filled with glycerol solution due to the chemical stability and non-toxicity. The base and PDMS film were created through molding. In a vacuum chamber, a 10:1 combination of PDMS monomer and curing agent was degassed for 15 min. The precursor was then poured into the corresponding specially made mold. The film and base can be demolded and filled with glycerol solution following a 40-min cure at a temperature of 80 °C. Finally, the PDMS film sandwiched with a fiber adapter was used to seal the liquid capsule. Thus, the optical fiber sensor was prepared. The soft, flexible PDMS film and base offer electric insulation and corrosion resistance for the sensor.

### Characterization of the proposed sensor

The static and dynamic response of the optical fiber sensor was systematically investigated. During the sensitivity test, a probe controlled by a three-dimensional micro displacement stage gradually compressed the sensor. The balance (JJ124BC) beneath the sensor simultaneously recorded the applied pressure with a resolution of 0.1 mg, while the optical power output of the sensor was recorded simultaneously by the optical power meter (PMSII-B). As Fig. 2(a) displayed, the proposed sensor exhibits decreasing power curves with applied pressure. The sensitivity is calculated using the slopes of the change in optical power ( $\Delta G$ ) vs the applied pressure ( $\Delta P$ ); the formula is  $S = (\Delta G)/(\Delta P)$ . The sensor displayed a sensitivity as  $-213 \mu\text{w}/\text{kPa}$  with a high linear working range of 0–2 kPa. Especially, the high linearity ( $R^2 = 0.989$ ) in this range is also exhibited, which helps to avoid distortion in pulse wave signals detection. It should be pointed out that the pulse wave signal is a weak pressure, thus sensors with a linear range of less than 2 kPa are sufficient for measuring pulse waves [20, 32]. To investigate the repeatability of sensitivity, five loading cycles are applied to the sensor. As Fig. 2(b) shown, five cycles present a high coincidence which means the sensor has a good consistency. Besides the sensitivity and consistency, the response time is also necessary for real-time vital signs monitoring. A ping pong ball fell freely to the sensor and promptly rebounded which induced a transient pulse of the sensor's output. As Fig. 2(c) presented, the rise time is only 5 ms, demonstrating the sensor is ultrafast in response and satisfies the real-time vital signs monitoring.

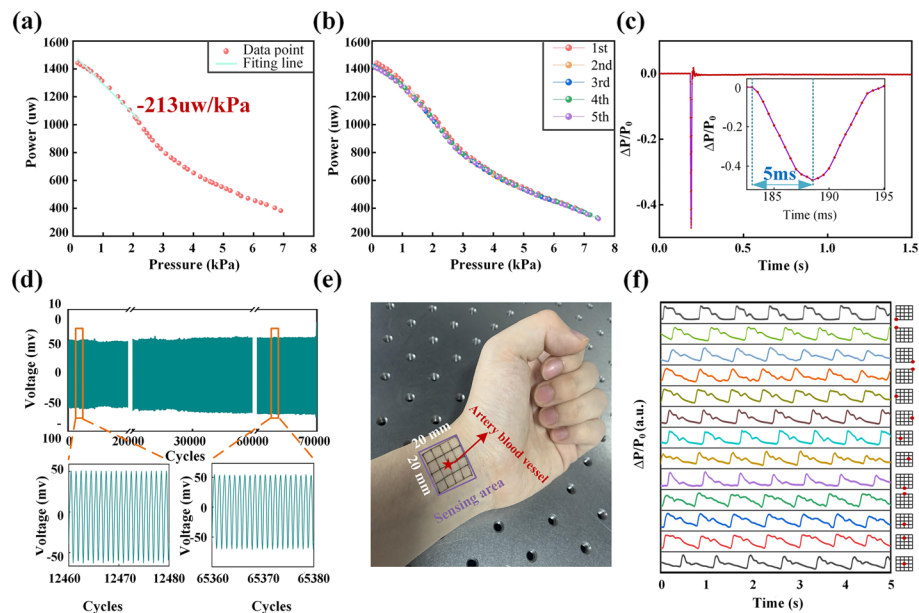


**Fig. 2** The characteristics of the optical fiber sensor. **a** The sensor's optical power-pressure curve, which ranges from 0–8 kPa. **b** Study of sensitivity coincidence over 5 cycles. **c** 70,000 cycles of cyclic loading at a frequency of 2 Hz are applied to the sensor. **d** Response time of the sensor. **e** The sensing area with sixteen grids on the wrist. **f** Arterial pulse signals from various sites by proposed sensor

To assess the operational stability and dependability over the long period, the proposed sensor was fixed to a three-dimensional micro displacement stage, and a vibration stage operating at a frequency of 10 Hz continuously supplied periodic pressure, as Fig. S1 investigated. Figure 2(d) shows that no obvious performance degradation was observed after 70,000 cycles, which indicates excellent robustness and durability. In addition, the sensor's dynamic response was further assessed at various frequencies between 10 and 40 Hz and the results are displayed in Fig. S2. It is obviously seen that under the high frequencies, the sensor shows no performance deterioration and continues to function flawlessly. It is hopeful that it will be evolved into a useful wearable gadget because of the long-lasting and repeatable performance.

To evaluate the free alignment and spatial insensitivity, the proposed sensor was placed at a different place in the wrist region to detect pulse signals. As Fig. 2(e) depicted, sixteen grids with an area of  $20 \times 20 \text{ mm}^2$  were marked in the radial artery region. The position of the arterial blood vessel has been indicated with a red star. The center of the sensor is aligned at different locations in the grid. Setting up a coordinate system will help to get a better understanding. The radial artery was set to the origin of the coordinates. The center of the sensor was placed on (0,0) (0,5) (0,-5) (0,10) (0,-10) (5,0) (-5,0) (10,0) (-10,0) (10,10) (10,-10) (-10,10) (-10,-10), respectively as depicted in Fig. 2(f) (Solid red circle). Obviously, there is no distortion of pulse wave signals caused by position drift which will ensure accuracy in blood pressure results. To further validate the liquid capsule performance, a fiber adapter was positioned at each grid point to collect signals, as displayed in Fig. S3. Compared with the proposed sensor, only when the fiber adapter was placed in close proximity to the radial artery, were undistorted pulse wave signals able to be successfully obtained. Thus, the proposed sensor held a number

of appealing qualities that made it ideal for long-term cardiovascular treatment, including great sensitivity, outstanding durability, and quick response time.

### **Pulse wave analysis and blood pressure monitoring**

During the whole ventricular pulsation, the heart contracts and relaxes continuously, leading to the expansion and contraction of the aortic vessel wall. Thus, the periodic increase and decrease of blood volume form the pressure changes in waves as pulse signals [33–37]. The pulse wave signals carry abundant cardiovascular information. The pulse wave signal's characteristics such as shape, period, peak value, and waveform feature are closely related to cardiovascular health levels [38, 39]. When pathological changes occur, the shape of the pulse wave will change accordingly. Thus, the features of pulse wave signals contain a wealth of physiological and pathological information about blood pressure. In this work, several blood pressure-related features were selected and analyzed. As presented in Fig. 3(a), The foot, the percussion wave peak, the dicrotic notch, and the dicrotic wave peak wave are all denoted by the letters "A," "B," "C," and "D," respectively. The detailed relationships and definitions are defined in Table 1.

Benefiting from the high sensitivity, fast responsiveness, high repeatability as well as conformability to the body, the smartwatch can be employed to measure pulse wave signals and estimate blood pressure by recording the dilation and contraction of blood vessels walls. Here, a machine learning technique was used to estimate the blood pressure, as demonstrated in Fig. 3(b). The pre-process was as follows: firstly, a low-pass filter with a cutoff frequency of 10 Hz was utilized to eliminate the noise brought on by high-frequency interference. Then the baseline drift caused by light intensity variation and other perturbations was eliminated via a polynomial method. Next, wavelet processing was used to increase the signal-to-noise ratio (SNR). The features of the pulse wave were extracted and then construct a trained model to estimate blood pressure values. The automatic correction threshold method is proposed to solve the misjudgment problem of feature points as presented in Fig. S4. A small initial threshold is set to identify whether the position of the dicrotic wave and dicrotic notch is misjudged, so as to automatically correct the threshold, and finally realize the adaptive extraction of the pulse wave points of different forms. This method can effectively solve the misjudgment problem of feature points. The Feature extraction based on automatic correction thresholding method will improve the accuracy of feature recognition, and increase the accuracy of blood pressure.

To establish a data set for the blood pressure estimation models, it was essential to precisely extract the features of the pulse wave signals, which will improve the accuracy and reduce overfitting. To further display the relationship between blood pressure values and features extracted from pulse wave signals, the Person correlation analysis was used to uncover the correlation coefficient [40]. Figure 3(c) and (d) plot the heat map of the Pearson correlation coefficient of SBP, DBP and pulse wave features, respectively. When two variables are positively correlated, the correlation coefficient is between 0 and 1, while negatively correlated, the correlation coefficient is between -1 and 0. It illustrates that the correlation coefficient between SBP and TmCA, TmBB, Area1, Area2, RSD, AmAB, AmAC are 0.80, 0.81, 0.66, 0.66, -0.66, -0.61, -0.70, respectively. As for DBP, the correlation coefficient between DBP and TmCA, TmBB, Area1, Area2, RSD,

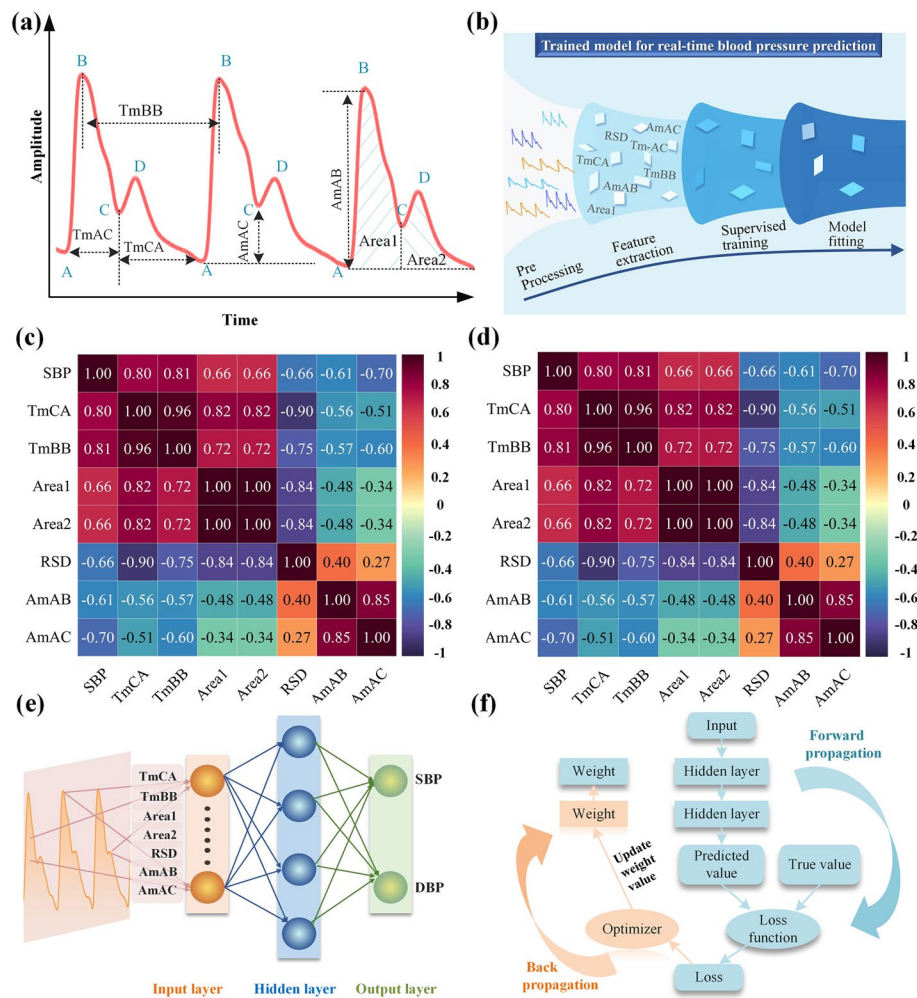


**Fig. 3** **a** Typical pulse wave signals with features defined. **b** Estimation process of the blood pressure. **c** Pearson correlation coefficients for the SBP's seven features. **d** Pearson correlation coefficient matrix between the seven DBP features. **e** The design of the supervised neural network. **f** The principle of Back Propagation Neural Network

**Table 1** Definitions of the selected features of pulse wave signals

Features	Definitions
AmAC	Amplitude between A peak and C peak
AmAB	Amplitude between A peak and B peak
TmBB	The time span between two successive A peaks
TmCA	The timespan between C peak of the current heartbeat and A peak of the next heartbeat
TmAC	The timespan between A peak and C peak of the same heartbeat
Area 1	Area of the systolic phase
Area 2	Area of the diastolic phase
RSD	The ratio of systole TmCA to diastole TmCA



AmAB, AmAC are 0.74, 0.64, 0.72, 0.72, -0.75, -0.56, -0.43, respectively. Especially, the two variables are considered to be significantly correlated when the correlation coefficient is greater than 0.6. Therefore, the seven features mentioned above were all selected to establish a data set for the SBP estimation models, TmCA, TmBB, Area1, Area2, and RSD were selected to establish a data set for the DBP estimation models.

### **Blood pressure estimation model based on machine learning**

Machine learning is considered a promising blood pressure estimation algorithm and it is expected to combine the extracted pulse wave features with it. The retrieved features in this instance served as inputs and produced two outputs that represented SBP and DBP. Back Propagation Neural Network (BPNN) was popularly used for blood pressure estimation because of its excellent generalization and adaptive ability [41–43]. A typical BPNN consists of the input layer, the hidden layer, and the output layer, as illustrated in Fig. 3(e). The principle of BPNN is shown in Fig. 3(f). When the network received a set of training samples, the activation values of the neurons propagated via the intermediate levels to the output layer. Each neuron in the output layer then received the network's input response. The second stage was the back-propagation of the error, from the output layer through each intermediate layer to correct each weight, and finally returned to the input layer. As the network continued to correct in the direction of decreasing error, the system's ability to respond to input accurately grew as well. In this work, a four-layer neural network that composed of an input layer, two hidden layers, and an output layer was constructed.

## **Results and discussion**

### **Blood pressure monitoring**

To validate the performance of the smartwatch for continuous blood pressure monitoring, we cooperated with the division of cardiology of hospital. The 105 sets of data were randomly selected for a practical experiment. Note that 70% of the dataset was used as the training set, while the remaining 30% was selected as the test set. Figure 4(a) and (b) plot the histogram distribution of the SBP and DBP dataset, respectively. During the measurement process, the volunteers kept silent and wore a smartwatch on their left-hand wrist to monitor blood pressure in real-time. To assess the precision of the measurement value, the intelligent sphygmomanometer (OMRON HEM-8102A) was worn on the upper arm of the right hand.

To fully evaluate the smartwatch's accuracy and precision, the error analysis was carried out. As shown in Table 2, the mean bias (Mean) and error standard deviation (SD) for SBP are determined as  $-0.35 \pm 4.68$  mmHg. For DBP, they are, respectively,  $-2.54$  mmHg and  $4.07$  mmHg. The Association for the Advancement of Medical Instrumentation (AAMI) states that standard deviations must be fewer than 8 mmHg and mean biases must be less than 5 mmHg [44]. Therefore, the smartwatch meets the requirements. Moreover, the British Hypertension Society (BHS) standard states that errors are commensurate with grade A [45]. The results of error analysis indicate that the smartwatch is well within the international standards.

Figure 4(c) and (d) present the measured blood pressure correlation analysis compared to the reference values. Here, the measured SBP and DBP were obtained from the testing data by using the Back Propagation Neural Network which was trained by using the training data. Also, the reference values were monitored by a commercial

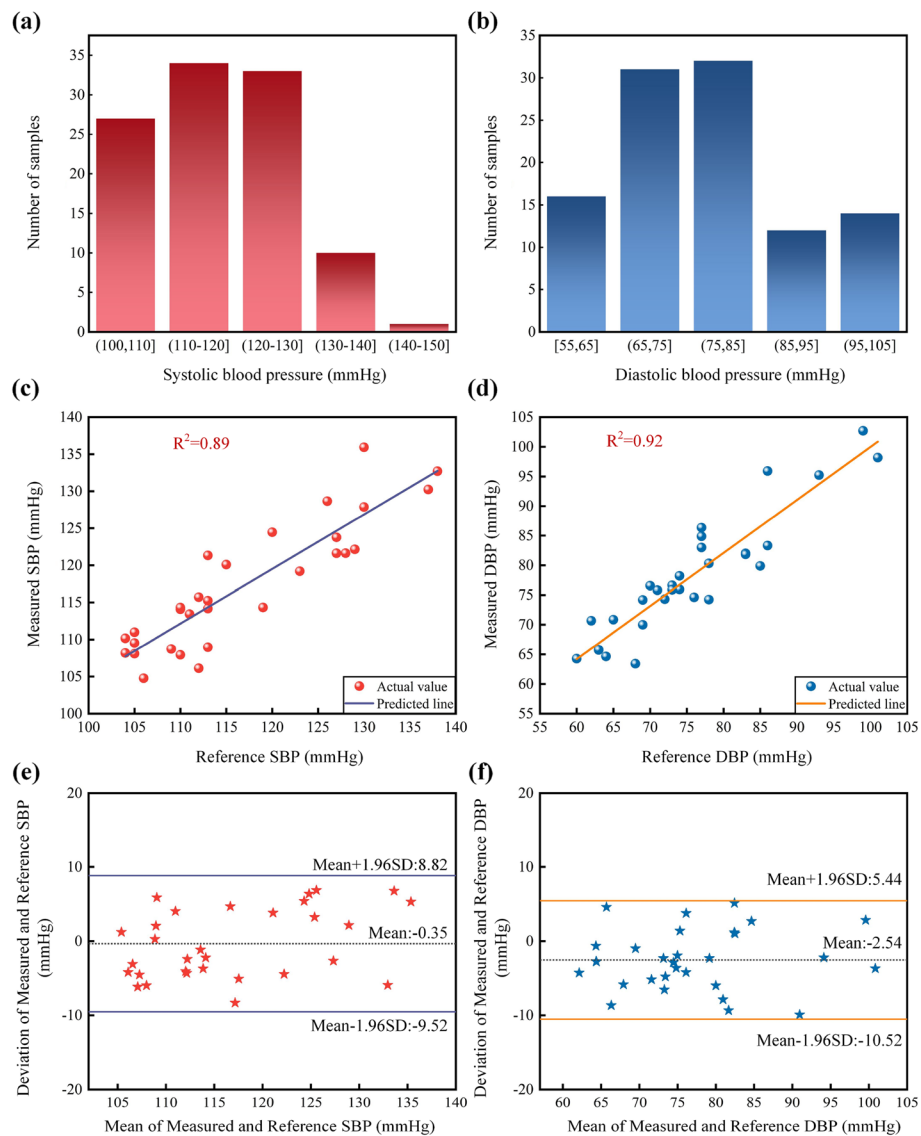


**Fig. 4** **a** Distribution of SBP. **b** Distribution of DBP. **c** Correlation analysis of systolic blood pressure by 30 subjects. **d** Correlation analysis of diastolic blood pressure by 30 subjects. **e** Bland–Altman plots of systolic blood pressure. **f** Bland–Altman plots of diastolic blood pressure

**Table 2** Results of blood pressure measurement

Blood pressure	Mean (mmHg)	SD (mmHg)
SBP	-0.35	4.68
DBP	-2.54	4.07

monitor. The estimated SBP and DBP correlation coefficients are 0.89 and 0.92, respectively, demonstrating that smartwatch correlates well with the reference sphygmomanometer. In addition, Bland–Altman analysis was used to evaluate the consistency of smartwatch and sphygmomanometer computing as Mean ± 1.96SD (Standard



**Fig. 5** **a** The smartwatch worn by a 25-year-old female. **b** The 24-h blood pressure variation. **c** The APP program

deviation) [46]. Bland-Altman recorded the deviation of two blood pressure values measured by smartwatch and sphygmomanometer, plotting it against the mean values at the same time. The Bland-Altman plots of SBP and DBP are illustrated in Fig. 4(e) and (f). For SBP, the mean blood pressure value is  $-0.35$  mmHg with a 95% confidence interval of  $-9.52$  mmHg to  $8.82$  mmHg and. Correspondingly, the 95% confidence interval is between  $-10.52$  mmHg to  $5.44$  mmHg and the mean blood pressure value is  $-2.54$  mmHg, for DBP. All results fall within the 95% confidence limits, suggesting that blood pressure values measured by the smartwatch are accurate and in complete agreement with the sphygmomanometer.

#### Ambulatory blood pressure monitoring

Compared with the current research which focused on the blood pressure sensors without integration [47–49], this work not only proposes a robust and sensitive sensor that eliminates the distortion of pulse signal caused by position drift and misalignment, but more importantly develops a wearable smartwatch integrated with essential elements. To demonstrate an application of ambulatory blood pressure monitoring, the proposed smartwatch was worn by a 25-year-old female as shown in Fig. 5(a), and the structure of a blood pressure smartwatch is illustrated in Figs. S5 and S6 displayed the accuracy of the smartwatch compare to a commercial sphygmomanometer. The SBP difference

between the proposed smartwatch and the commercial sphygmomanometer is 0 while the DBP difference is 4 mmHg. The results of the error analysis indicate that the smartwatch is well within international standards. The blood pressure data from 8:00 in the morning to 8:00 the next day was continuously recorded. It can be observed from Fig. 5(b) that blood pressure has the lowest value at night (2:00 am) and rises rapidly after getting up in the morning, then a peak at 6–10 am and 4–8 pm will appear, followed by a slow decline. To further improve user-friendliness, a customized APP program was developed as exhibited in Fig. 5(c). The personal information interface, a 24-h historical data interface, a real-time measurement interface, and a week historical data interface were displayed to realize capture and analysis of health data in real-time. In addition, it is significant to assist patients with hypertension recording their condition as a reference for medication. As such, the proposed smartwatch provides digital and personalized health monitoring.

## Conclusion

In general, we have demonstrated a unique flexible high-performance optical fiber sensor and integrated it with a smartwatch to achieve automatic and accurate blood pressure monitoring. Combining the advantages of the fiber adapter and the liquid capsule, the sensor can perform effective measurement of pulse wave signals. Besides excellent performance, such as robust sensitivity ( $-213 \mu\text{w}/\text{kPa}$ ), fast dynamical response ( $< 5 \text{ ms}$ ), and high stability ( $> 70,000$  cycles), high-fidelity pulse wave signals in the region of  $20 \times 20 \text{ mm}^2$  are obtained while the distortion caused by position misalignment was eliminated. This work not only designs an optical fiber sensor but more importantly extends the sensing area and integrates it into a smartwatch. By extracting the features of pulse waves using the automatic correction threshold method and constructing a BPNN estimation model, blood pressure values can be accurately calculated. The errors of SBP and DBP were  $-0.35 \pm 4.68 \text{ mmHg}$  and  $-2.54 \pm 4.07 \text{ mmHg}$ , respectively, which were within the international standard. Furthermore, a wearable smartwatch integrated with a signal processing chip, a Bluetooth transmission module, and a specially designed mobile APP was developed to monitor 24-h blood pressure. This work constitutes the breakthrough for ambulatory personalized blood pressure monitoring as well as active daily human health management.

## Abbreviations

AAMI	Association for the Advancement of Medical Instrumentation.
BHS	British Hypertension Society
PPG	Photoplethysmogram
EMI	Electromagnetic interferences
FTTH	Fiber To The Home
(FBG)	Fiber Bragg Gratings
SMS	Singlemode-Multimode-Singlemode
PTT	Pulse transit time
SBP	Systolic blood pressure
DBP	Diastolic blood pressure
PE	Polyethylene
UV	Ultraviolet
FEA	Finite-elemental analysis
PDMS	Polydimethylsiloxane
SNR	Signal-to-noise ratio
BPNN	Back Propagation Neural Network
Mean	The mean bias
SD	Error standard deviation

## Supplementary Information

The online version contains supplementary material available at <https://doi.org/10.1186/s43074-023-00099-z>.

Additional file 1.

### Acknowledgements

Not applicable at this moment.

### Authors' contributions

Q.S. and P.S. conceived the project. L.L., Y.L., and Z.C. fabricated the device. L.L., S.S., and J.W. carried out the data collection. L.L. and Q.S. wrote the paper. C.C., W.F., Z.Z. and W.X. participated the discuss of results, with all authors contributing to the discussion and preparation of the manuscript.

### Funding

We are grateful for financial support from the National Science Fund of China for Excellent Young Scholars (No. 61922033) and the Fundamental Research Funds for the Central Universities (HUST: YCJJ202201002).

### Availability of data and materials

The data and the relevant methods are available on request from the corresponding authors.

### Declarations

#### Ethics approval and consent to participate

There is no ethics issue for this paper.

#### Consent for publication

All authors agreed to publish this paper.

#### Competing interests

There are no competing interests for this paper.

Received: 9 March 2023 Revised: 24 May 2023 Accepted: 19 June 2023

Published online: 03 July 2023

### References

1. Ma L-Y, Chen W-W, Gao R-L, Liu L-S, Zhu M-L, Wang Y-J, Wu Z-S, Li H-J, Gu D-F, Yang Y-J. China cardiovascular diseases report 2018: an updated summary. *J Geriatr Cardiol.* 2020;17:1.
2. Radovanovic CAT, Santos LAd, Carvalho MDdB, Marcon SS. Arterial Hypertension and other risk factors associated with cardiovascular diseases among adults. *Revista latino-americana de enfermagem.* 2014;22: 547–553.
3. Liu S, Li Y, Zeng X, Wang H, Yin P, Wang L, Liu Y, Liu J, Qi J, Ran S. Burden of cardiovascular diseases in China, 1990–2016: findings from the 2016 global burden of disease study. *JAMA Cardiol.* 2019;4:342–52.
4. Allender S, Scarborough P, Peto V, Rayner M, Leal J, Luengo-Fernandez R, Gray A. European Heart. Network. 2008;3:11–35.
5. Zhou B, Carrillo-Larco RM, Danaei G, Riley LM, Paciorek CJ, Stevens GA, Gregg EW, Bennett JE, Solomon B, Singleton RK. Worldwide trends in hypertension prevalence and progress in treatment and control from 1990 to 2019: a pooled analysis of 1201 population-representative studies with 104 million participants. *Lancet.* 2021;398:957–80.
6. Imai Y, Sasaki S, Minami N, Munakata M, Hashimoto J, Sakuma H, Sakuma M, Watanabe N, Imai K, Sekino H. The accuracy and performance of the A&D TM 2421, a new ambulatory blood pressure monitoring device based on the cuff-oscillometric method and the Korotkoff sound technique. *Am J Hypertens.* 1992;5:719–26.
7. Geddes L, Voelz M, Combs C, Reiner D, Babbs CF. Characterization of the oscillometric method for measuring indirect blood pressure. *Ann Biomed Eng.* 1982;10:271–80.
8. Chan G, Cooper R, Hosanee M, Welykholowa K, Kyriacou PA, Zheng D, Allen J, Abbott D, Lovell NH, Fletcher R. Multi-site photoplethysmography technology for blood pressure assessment: challenges and recommendations. *J Clin Med.* 2019;8:1827.
9. Xing X, Sun M. Optical blood pressure estimation with photoplethysmography and FFT-based neural networks. *Biomed Opt Express.* 2016;7:3007–20.
10. Allen J. Photoplethysmography and its application in clinical physiological measurement. *Physiol Meas.* 2007;28:R1.
11. Ma Y, Zheng Q, Liu Y, Shi B, Xue X, Ji W, Liu Z, Jin Y, Zou Y, An Z. Self-powered, one-stop, and multifunctional implantable triboelectric active sensor for real-time biomedical monitoring. *Nano Lett.* 2016;16:6042–51.
12. Fang Y, Zou Y, Xu J, Chen G, Zhou Y, Deng W, Zhao X, Roustaei M, Hsiai TK, Chen J. Ambulatory cardiovascular monitoring via a machine-learning-assisted textile triboelectric sensor. *Adv Mater.* 2021;33:2104178.
13. Cheng X, Xue X, Ma Y, Han M, Zhang W, Xu Z, Zhang H, Zhang H. Implantable and self-powered blood pressure monitoring based on a piezoelectric thinfilm: simulated, in vitro and in vivo studies. *Nano Energy.* 2016;22:453–60.
14. Kaniusas E, Pftzner H, Mehnen L, Kosel J, Tellez-Blanco C, Varoneckas G, Alonderis A, Meydan T, Vázquez M, Rohn M. Method for continuous noninvasive monitoring of blood pressure by magnetoelastic skin curvature sensor and ECG. *IEEE Sens J.* 2006;6:819–28.
15. Kim K-H, Hong SK, Jang N-S, Ha S-H, Lee HW, Kim J-M. Wearable resistive pressure sensor based on highly flexible carbon composite conductors with irregular surface morphology. *ACS Appl Mater Interfaces.* 2017;9:17499–507.
16. Lo LW, Shi H, Wan H, Xu Z, Tan X, Wang C. Inkjet-printed soft resistive pressure sensor patch for wearable electronics applications. *Adv Funct Mater.* 2020;5:1900717.

17. Rao KS, Samyuktha W, Vardhan DV, Naidu BG, Kumar PA, Sravani KG, Guha K. Design and sensitivity analysis of capacitive MEMS pressure sensor for blood pressure measurement. *Microsyst Technol.* 2020;26:2371–9.
18. Kim J, Chou EF, Le J, Wong S, Chu M, Khine M. Soft wearable pressure sensors for beat-to-beat blood pressure monitoring. *Adv Funct Mater.* 2019;8:1900109.
19. Wang C, Li X, Hu H, Zhang L, Huang Z, Lin M, Zhang Z, Yin Z, Huang B, Gong H. Monitoring of the central blood pressure waveform via a conformal ultrasonic device. *Nat Biomed Eng.* 2018;2:687–95.
20. Zhang L, Pan J, Zhang Z, Wu H, Yao N, Cai D, Xu Y, Zhang J, Sun G, Wang L. Ultrasensitive skin-like wearable optical sensors based on glass micro/nanofibers. *Opto-Electron. Adv.* 2020;3:190022–1–190022–7.
21. Guo J, Zhou B, Zong R, Pan L, Li X, Yu X, Yang C, Kong L, Dai Q. Stretchable and highly sensitive optical strain sensors for human-activity monitoring and healthcare. *ACS Appl Mater Interfaces.* 2019;11:33589–98.
22. Tang Y, Liu H, Pan J, Zhang Z, Xu Y, Yao N, Zhang L, Tong L. Optical Micro/Nanofiber-Enabled Compact Tactile Sensor for Hardness Discrimination. *ACS Appl Mater Interfaces.* 2021;13:4560–6.
23. Guo J, Liu X, Jiang N, Yetisen AK, Yuk H, Yang C, Khademhosseini A, Zhao X, Yun SH. Highly stretchable, strain sensing hydrogel optical fibers. *Adv Mater.* 2016;28:10244–9.
24. Park S-J, Lee C-H, Jeong K-T, Park H-J, Ahn J-G, Song K-H. Fiber-to-the-home services based on wavelength-division-multiplexing passive optical network. *J Lightwave Technol.* 2004;22:2582.
25. Zhu HT, Zhan LW, Dai Q, Xu B, Chen Y, Lu YQ, Xu F. Self-Assembled Wavy Optical Microfiber for Stretchable Wearable Sensor. *Adv Opt Mater.* 2021;9:2002206.
26. Haseda Y, Bonafacio J, Tam H-Y, Chino S, Koyama S, Ishizawa H. Measurement of pulse wave signals and blood pressure by a plastic optical fiber FBG sensor. *Sensors.* 2019;19:5088.
27. Pang Y-N, Liu B, Liu J, Wan S, Wu T, Yuan J, Xin X, He XD, Wu Q. Singlemode-multimode-singlemode optical fiber sensor for accurate blood pressure monitoring. *J Lightwave Technol.* 2022;40:4443–50.
28. Fan X, Huang Y, Ding X, Luo N, Li C, Zhao N, Chen SC. Alignment-free liquid-capsule pressure sensor for cardiovascular monitoring. *Adv Funct Mater.* 2018;28:1805045.
29. Fuard D, Tzvetkova-Chevolleau T, Decossas S, Tracqui P, Schiavone P. Optimization of poly-di-methyl-siloxane (PDMS) substrates for studying cellular adhesion and motility. *Microelectron Eng.* 2008;85:1289–93.
30. Mata A, Fleischman AJ, Roy S. Characterization of polydimethylsiloxane (PDMS) properties for biomedical micro/nanosystems. *Biomed Microdevices.* 2005;7:281–93.
31. Regehr KJ, Domenech M, Koepsel JT, Carver KC, Ellison-Zelski SJ, Murphy WL, Schuler LA, Alarid ET, Beebe DJ. Biological implications of polydimethylsiloxane-based microfluidic cell culture. *Lab Chip.* 2009;9:2132–9.
32. Yan H, Wang Y, Fufeng L, Gong A, Yun F, Hong Y, Jin X, Cheng Y, Lei H, Zhaoxia X. Relationship of optimal pulse-taking pressure among cun, guan, chi pulse of 264 healthy undergraduates. *China Journal of Traditional Chinese Medicine and Pharmacy.* 2006.
33. Wang J, Liu K, Sun Q, Ni X, Ai F, Wang S, Yan Z, Liu D. Diaphragm-based optical fiber sensor for pulse wave monitoring and cardiovascular diseases diagnosis. *J Biophotonics.* 2019;12: e201900084.
34. Song Z, Li W, Bao Y, Wang W, Liu Z, Han F, Han D, Niu L. Bioinspired microstructured pressure sensor based on a janus graphene film for monitoring vital signs and cardiovascular assessment. *Adv Electron Mater.* 2018;4:1800252.
35. Fu Y, Zhao S, Wang L, Zhu R. A wearable sensor using structured silver-particle reinforced PDMS for radial arterial pulse wave monitoring. *Adv Healthc Mater.* 2019;8:1900633.
36. Liu Y, Meng F, Zhou Y, Mugo SM, Zhang Q. Graphene oxide films prepared using gelatin nanofibers as wearable sensors for monitoring cardiovascular health. *Adv Mater Technol-US.* 2019;4:1900540.
37. Sun Y, Dong Y, Gao R, Chu Y, Zhang M, Qian X, Wang X. Wearable pulse wave monitoring system based on MEMS sensors. *Micromachines.* 2018;9:90.
38. Li Y, Wang Z, Zhang L, Yang X, Song J. Characters available in photoplethysmogram for blood pressure estimation: beyond the pulse transit time. *Phys Eng Sci Med.* 2014;37:367–76.
39. Li L, Liu Y, Song C, Sheng S, Yang L, Yan Z, Hu DJJ, Sun Q. Wearable alignment-free microfiber-based sensor chip for precise vital signs monitoring and cardiovascular assessment. *Adv Fiber Mater.* 2022;4:475–86.
40. Zeng Z, Huang Z, Leng K, Han W, Niu H, Yu Y, Ling Q, Liu J, Wu Z, Zang J. Noninvasive monitoring of mental fatigue status using epidermal electronic systems and machine-learning algorithms. *ACS Sens.* 2020;5:1305–13.
41. Xu Z, Liu J, Chen X, Wang Y, Zhao Z. Continuous blood pressure estimation based on multiple parameters from electrocardiogram and photoplethysmogram by Back-propagation neural network. *Comput Ind.* 2017;89:50–9.
42. Chen C-T, Lin W-L, Kuo T-S, Wang C-Y. Adaptive control of arterial blood pressure with a learning controller based on multilayer neural networks. *IEEE Trans Biomed Eng.* 1997;44:601–9.
43. Wang J-Z, Wang J-J, Zhang Z-G, Guo S-P. Forecasting stock indices with back propagation neural network. *Expert Syst Appl.* 2011;38:14346–55.
44. Luo H, Yang D, Barszczyk A, Vempala N, Wei J, Wu SJ, Zheng PP, Fu G, Lee K, Feng Z-P. Smartphone-based blood pressure measurement using transdermal optical imaging technology. *Cardiovascular Imaging.* 2019;12: e008857.
45. O'Brien E, Petrie J, Littler W, de Swiet M, Padfield PL, Altman D, Bland M, Coats A, Atkins N. The British Hypertension Society protocol for the evaluation of blood pressure measuring devices. *J Hypertens.* 1993;11:543–62.
46. Bland JM, Altman D. Statistical methods for assessing agreement between two methods of clinical measurement. *1986;327:307–10.*
47. Kao Y-H, Tu T-Y, Chao PC-P, Lee Y-P, Wey C-L. Optimizing a new cuffless blood pressure sensor via a solid–fluid–electric finite element model with consideration of varied mis-positionings. *Microsystem Technologies.* 2016;22:1437–1447.
48. Koyama S, Ishizawa H, Fujimoto K, Chino S, Kobayashi Y. Influence of individual differences on the calculation method for FBG-type blood pressure sensors. *Sensors.* 2016;17:48.
49. Wang T-W, Lin S-F. Wearable piezoelectric-based system for continuous beat-to-beat blood pressure measurement. *Sensors.* 2020;20:851.

## Publisher's Note

Springer Nature remains neutral with regard to jurisdictional claims in published maps and institutional affiliations.